JACS
JOURNAL OF THE AMERICAN CHEMICAL SOCIETY

Article

pubs.acs.org/JACS

Insights into the Mechanism of Proton Transport in Cytochrome *c* Oxidase

Takefumi Yamashita† and Gregory A. Voth*

Department of Chemistry, James Franck Institute, Institute for Biophysical Dynamics, and Computation Institute, University of Chicago, 5735 S. Ellis Ave., Chicago, Illinois 60637, United States

Supporting Information

ABSTRACT: Cytochrome *c* oxidase (CcO), known as complex IV of the electron transport chain, plays several important roles in aerobic cellular respiration. Electrons transferred from cytochrome *c* to CcO's catalytic site reduce molecular oxygen and produce a water molecule. These electron transfers also drive active proton pumping from the matrix (N-side) to intermembrane region (P-side) in mitochondria; the resultant proton gradient activates ATP synthase to produce ATP from ADP. Although the existence of the coupling between the electron transfer and the proton transport (PT) is established experimentally, its mechanism is not yet fully understood at the molecular level. In this work, it is shown why the reduction of heme a is essential for proton pumping. This is demonstrated via novel reactive molecular dynamics (MD) simulations that can describe the Grotthuss shuttling associated with the PT as well as the dynamic delocalization of the excess proton electronic charge defect. Moreover, the "valve" role of the Glu242 residue (bovine CcO notation) and the gate role of D-propionate of heme a_3 (PRDa3) in the explicit PT are explicitly demonstrated for the first time. These results provide conclusive evidence for the CcO proton transporting mechanism inferred from experiments, while deepening the molecular level understanding of the CcO proton switch.

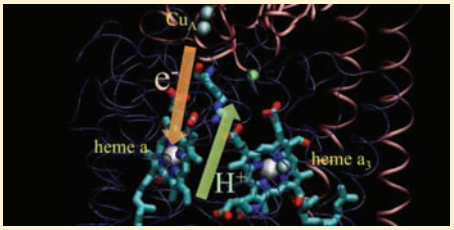

1. INTRODUCTION

The proton pumping mechanism of cytochrome *c* oxidase (CcO)[1−4] is a very important process, because the resultant proton gradient is the driving force behind the production of ATP. The proton translocation is driven by the electron transfer inside CcO: One current model[1−3] says that cytochrome *c* reduced by cytochrome bc_1 complex (complex III) first carries an electron to Cu_A, located in subunit II (SU-II) of CcO (see Figure 1). The electron transfers to heme a and then to the binuclear center (BNC) consisting of heme a_3 and Cu_B, all of which are included in subunit I (SU-I). The BNC is the sink of the transferred electron and also the catalytic site that reduces an oxygen molecule to a water molecule. Note that a single catalytic turnover involves four proton pumping processes, each of which is associated with a reaction where one electron and one proton are added to the catalytic site. The nonpolar cavity between heme a and the BNC is connected to the matrix side (N-side) by two proton pathways, the so called D- and K-channels. These channels are observed in the X-ray crystal structures[5,6] and found to be the proton pathways by site-directed mutation experiments,[1] although the proton exit pathway to the intermembrane region (P-side) has not yet been established.

Based on the characteristic structures, it is natural to expect that a proton switch, which must be sensitive to the CcO oxidation state, should be involved around the nonpolar cavity. Mitchell and Rich[7] proposed the electroneutrality principle, which assumes that the proton uptake to the nonpolar cavity neutralizes the charge around the nonpolar cavity due to the electrostatic attraction present soon after the electron arrives at the heme groups. According to this principle, as well as numerous experimental results, several catalytic cycle mechanisms of CcO have been proposed.[3,4,8] Recently, a kinetic analysis was also performed in order to investigate possible proton pumping mechanisms of CcO systematically.[9]

Experimentally, Faxén et al.[10] suggested that the proton release is mechanistically coupled with the proton transfer to the BNC but not with the electron transfer. Shortly thereafter, Belevich et al.[11] discovered the vectorial charge movement during the $A \rightarrow P_R$ transition, which involves the electron transfer from heme a to the BNC. The amount of the transferred charge is estimated to be the value that one charge transfers across 30% of the membrane dielectric. Based on these results, Wikström and co-workers[3,11,12] proposed a proton pumping mechanism illustrated in Figure 2. That being said, there is relatively little molecular level proof for this mechanism, and it is particularly unclear how the change of the oxidation states drives the proton transport (PT).

One means of obtaining molecular level information is to perform molecular dynamics (MD) simulations. Thus far, standard MD simulations have elucidated the significant effects of the oxidation state change on both the hydrogen-bond network of the water cluster inside the nonpolar cavity[13] and the Arg438−PRDa3 ion pair.[14] However, no explicit information on the PT was extracted from the simulations,

Received: September 29, 2011
Published: December 19, 2011

dx.doi.org/10.1021/ja209176e | J. Am. Chem.Soc. 2012, 134, 1147−1152

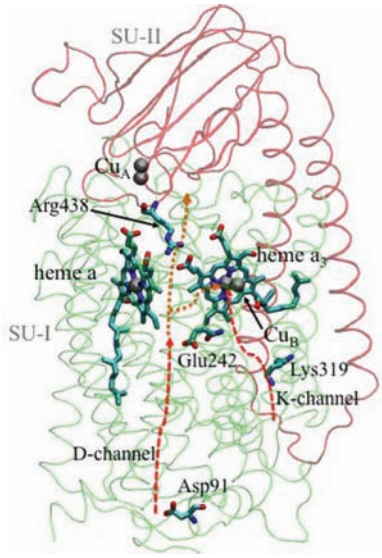

Figure 1. Structure of CcO (bovine). The main functional groups of CcO are located in SU-I and SU-II. Whereas Cu_A is located in SU-II, the other redox centers are in SU-I. The K-channel connects the BNC and Lys319, and the D-channel starts from Asp91 and terminates at Glu242. Above Glu242, there is the nonpolar cavity, which is surrounded by two heme groups. Whereas all the K-channel protons are used as chemical protons, both chemical protons and pumped protons are transported through the D-channel. The K-channel is open only in the reductive phase. PRDa3 forms an ion contact pair with Arg438.

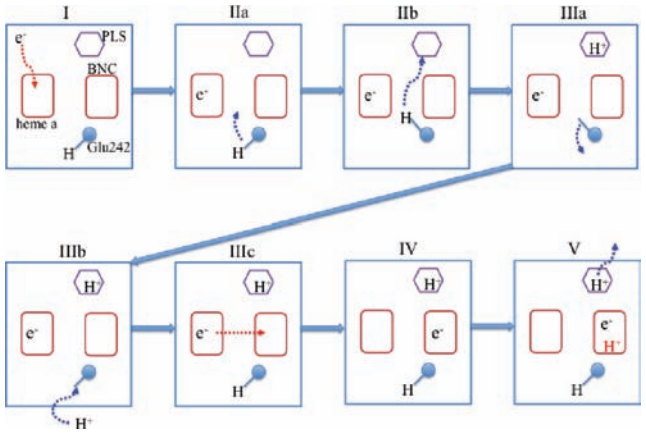

Figure 2. Proposed proton pumping mechanism (ref 12). Reduction of heme a (I → IIa) helps Glu242 to turn up toward the nonpolar cavity (IIa → IIb), which leads the first proton transport from Glu242 to the PLS (IIb → IIIa). Deprotonated Glu242 turns down toward the D-channel (IIIa → IIIb) and accepts another proton (IIIb → IIIc). Then, the electron transfers from heme a to heme a_3 (IIIc → IV), and the proton uptake occurs through the D-channel in the oxidative phase and through the K-channel in the reductive phase (IV → V). This proton is pictured in red only in step V. Note that step I corresponds to the OO state (where both heme a and heme a_3 are oxidized), steps IIa–IIIc correspond to the RO state (where heme a is reduced but heme a_3 is oxidized), and steps IV–V correspond to the OR state (where heme a is oxidized but heme a_3 is reduced).

because standard empirical force fields cannot describe the PT process.[15−17] The purpose of this work is to therefore investigate the oxidation state dependence of the explicit PT in the nonpolar cavity and to provide information about the underlying molecular level mechanism of the proton pumping function of CcO using a novel reactive MD method.[16,17] For this purpose, an excess proton in the CcO environment is explicitly simulated in this work in order to calculate the free energy change driving the PT in the nonpolar cavity. It will be explicitly shown that the nonpolar cavity region can act as a proton switch with a large oxidation state dependence.

2. METHODS

The difficulty in simulating the excess proton is caused by the excess charge defect delocalization and the bond alternation mechanism associated with the Grotthuss proton shuttling.[15] In this work, the multistate empirical valence bond (MS-EVB) reactive MD method[16,17] is utilized because it can correctly describe the excess proton shuttling behavior in aqueous and biomolecular environments and its computational cost is significantly lower than that of ab initio MD or semiempirical methods. These advantages make it possible to perform statistically converged free energy analysis of the excess proton behavior.

It should be noted that, due to Grotthuss shuttling, one cannot assign a specific hydrogen nucleus to the "excess proton". Thus, to describe the position of the protonic charge defect, the center of excess charge (CEC) is adopted in this paper.[16,17] (See Section 3 of the Supporting Information.) The origin of the space-fixed Cartesian coordinates is located at the position of the δ-carbon of Glu242 in the crystal structure. (In this work, the PDB entry 1V54 was employed.[18]) Then, this δ-carbon is observed to fluctuate around $z = 0$ in the MD simulations when Glu242 is in the down conformation. The z coordinate is defined to point from the N-side to the P-side.

Reduced CcO models consisting only of SU-I and SU-II [denoted as CcO(I+II)] were used in this work to lower the computational cost. These models can be considered reasonable because all of the important moieties are included in SU-I and SU-II. In fact, it has been experimentally shown that the proton pumping function is maintained in the absence of SU-III, although the pumping becomes slower.[19] To investigate the oxidation state dependence of the PT, potentials of mean force (PMFs) are calculated to provide the PT free energy profiles for three different oxidation states: OO, RO, and OR. Both heme a and heme a_3 are oxidized (+III) in OO, while heme a is reduced (+II) and heme a_3 is oxidized in RO, and heme a is oxidized and heme a_3 is reduced in OR. The OO, RO, and OR states correspond to stages I, II–III, and IV–V, respectively (see Figure 2). Note that Cu_A is oxidized and Cu_B is reduced in this work.

The PMFs were calculated with the umbrella sampling technique[20,21] in which the z coordinate of the excess proton CEC is biased by a harmonic umbrella potential. All of the simulations in this work were performed using the following procedure: First, the sixth ligand of heme a_3 and five additional water molecules were added to the nonpolar cavity region of CcO. Note that either H_2O or OH^- is employed as the sixth ligand of heme a_3 here. After the system was equilibrated sufficiently, the water molecule that has the greatest proximity to Glu242 in the nonpolar cavity was replaced by a hydronium cation. Then, the system with the excess proton was equilibrated with an umbrella potential, limiting the CEC around the initial point. After that, the center of the umbrella potential was slightly shifted, and the system equilibrated again. By doing this procedure iteratively, the initial conditions for all of the umbrella sampling windows were generated. Once the equilibrated initial conditions were obtained, an MD trajectory was run for 1 ns in each window in order to obtain the overall PMF. Figure 3 shows several umbrella sampling MD snapshots to visualize the vectorial proton pathway.

The proton-loading site (PLS), which is considered to be located just above Glu242, has not yet been conclusively determined, although the crystal structures of CcO[5,6] imply that four propionates of the two heme groups are candidates for the PLS. (His291 is another candidate, but Fadda, Chakrabarti, and Pomès[22] have suggested this is unlikely based on the quantum chemical calculations in combination with continuum electrostatics.) As shown in Figure 3, PRDa3 is involved in the proton exit pathway and seems to transfer the proton to A-propionate of heme a_3 (PRAa3). This result is consistent with the

dx.doi.org/10.1021/ja209176e | J. Am. Chem.Soc. 2012, 134, 1147–1152

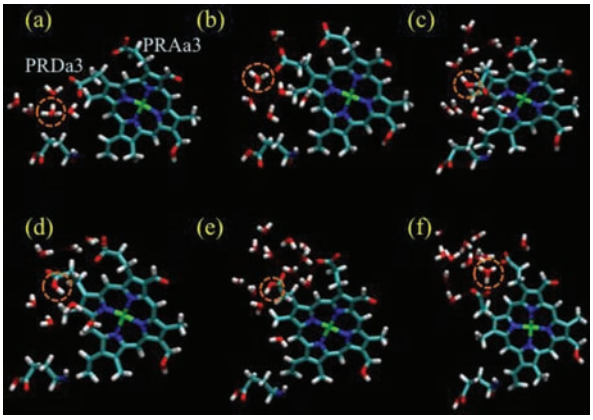

Figure 3. Vectorial proton pathway from the nonpolar cavity toward the hydrophilic region above it in the RO state for simulation snapshots taken from that region of the first model. Orange circles highlight the most protonated species, and the excess proton CECs are located at (a) z_{CEC} = 4.1, (b) 6.9, (c) 7.4, (d) 8.4, (e) 10.5, and (f) 13.0 Å. (In this paper, z_{CEC} is the z coordinate of the excess proton CEC.) Torsional rotation of PRDa3 and proton pumping occur cooperatively. PRDa3 turns down to the nonpolar cavity so as to coordinate the hydrated excess proton. After PRDa3 is protonated, the PRDa3 turns up to the hydrophilic region and ejects the proton. Finally, the hydrated proton is solvated by both of PRDa3 and PRAa3.

hypothesis that PRAa3 is a main part of the PLS, which is also supported by the results from an electrostatic analysis based on the pK_a shift of the PLS caused by the oxidation state change,[3] from a quantum chemical analysis,[23] and from empirical MD simulations.[24] In addition, in a recent QM/MM study, it was assumed that PRAa3 is involved in the proton exit pathway.[25]

It should be noted that two other computational methods were recently applied to study the energetics of PT in the nonpolar cavity of CcO; one is the semiempirical self-consistent charge-density functional tight binding (SCC-DFTB) method utilized by Ghosh et al.[26] and the other is a simpler and thus more approximate EVB method utilized by Warshel and co-workers.[27−29] However, the SCC-DFTB method was recently shown to yield inaccurate descriptions of both liquid water and the hydrated excess proton in water.[30,31] Also, the simpler EVB method, which often relies on a two-state description, is often not able to describe the hydrated excess proton naturally in complex aqueous and biomolecular environments.[16,17,32] In addition, although the conformations of the key residues and the water cluster inside the nonpolar cavity were constrained in these simulations,[27−29] as shown later, the conformational changes depending on the oxidation state of the heme groups and the water dynamics associated with the PT inside the nonpolar cavity play important roles in the proton pumping function of CcO.

3. RESULTS AND DISCUSSION

3.1. H_2O-Bound CcO with Protonated Glu242. The first system studied was the CcO(I+II) model that binds a water molecule as the sixth ligand of heme a_3. Here, Glu242 was protonated, which assumes a limiting case in which a rapid reprotonation happens shortly after Glu242 ejects a proton into the nonpolar cavity. The question of when Glu242 is reprotonated will be discussed later in the light of the possible valve role of Glu242.[33] Note that PRDa3 is modeled here in the MS-EVB reactive MD framework to allow PRDa3 to be dynamically protonated or deprotonated in the MD simulations (see section three of the Supporting Information).

Figure 4 shows the resultant PT PMFs for the three different oxidation states. The minima located around z_{CEC} = 7 Å correspond to the structures in which PRDa3 is protonated

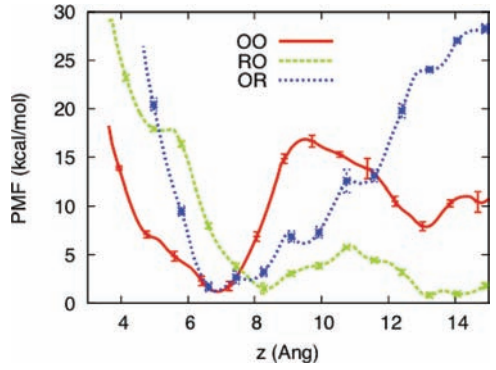

Figure 4. PT free energy profiles (PMFs) as functions of the z coordinate of the excess proton CEC for the first CcO model. (Glu242 is protonated and the BNC binds a water molecule.) The PT free energy barrier is significantly lower in the RO state than in the other two states.

inside the nonpolar cavity, as shown in Figure 3. As z_{CEC} increases, PRDa3 turns up toward the P-side. At $z_{CEC} \approx 12$ Å, the excess proton fully escapes from the nonpolar cavity region to the hydrophilic region above heme a_3. The OO state has a 15 kcal/mol barrier at $z_{CEC} \approx 9.5$ Å, whereas the PMF increases monotonically for the OR state due to the lack of an effective proton acceptor.

In contrast to the OO and OR oxidation states, the PT barrier height of the RO state is less than 5 kcal/mol, and the proton in the hydrophilic region located above heme a_3 is significantly stabilized. Importantly, this result agrees with the proton pumping mechanism proposed by Wikström and co-workers,[3,11,12] since the corresponding stage, IIa−IIIc in Figure 2, is considered to involve the PT from Glu242 to the PLS.

The clear sensitivity of the excess proton behavior to the oxidation state change originates from the change of the electrostatic field generated by heme a and heme a_3. However, it likely does not involve the direct interaction between the excess proton and the two heme groups, because this interaction is almost perpendicular to the proton pumping direction (z direction). Instead, it is of greater significance that the hydrogen-bond network is largely affected by the oxidation state change in its structural and dynamical aspects. For example, a characteristic hydrogen-bond chain connecting the excess proton and the BNC can be observed in the OO and OR states but not in the RO state (see Section 1 of the Supporting Information). In the state corresponding to OR in the oxidative phase of the CcO catalytic cycle, such a chain will play an important role in conducting a chemical proton to the BNC. The recent FTIR experiment also confirmed that the hydrogen-bond network rearrangement occurs in response to the oxidation state change.[34] Also, Wikström et al. reported that the hydrogen-bond network of the water cluster in the nonpolar cavity is changed by change of oxidation states of heme a and the BNC, although their empirical MD simulations included no excess proton.[13]

It is also observed that the dependence of the PMF on the oxidation state is considerably less in a smaller CcO model consisting of only SU-I [denoted as CcO(I)] as well as another CcO(I+II) model with unprotonatable PRDa3 (see Section 2 of the Supporting Information and the earlier paper of Xu and Voth[35] for comparison). The behavior of these two simpler models is likely due to the fact that these models cannot describe the change of the hydrogen-bond network sufficiently.

dx.doi.org/10.1021/ja209176e | J. Am. Chem.Soc. 2012, 134, 1147−1152

While it may be evident that an inability of PRDa3 to be protonated can considerably affect the hydrogen-bond network, it is also clear that the absence of SU-II can also cause a significant change in that network. Possible reasons for this are the electrostatic interaction with SU-II, the flexibility of motion of several residues located at the interface between SU-I and SU-II (e.g., Asp438), and an unrealistic invasion of the water molecule from the upper hydrophilic region to the nonpolar cavity in the smaller CcO(I) model (see Figure S6 of the Supporting Information for the latter behavior). This also points to an important additional role played by SU-II, that is, a contribution to the important structure of the water molecules for PT in CcO.

3.2. H_2O-Bound CcO with Deprotonated Glu242. In order to consider the other limiting case that Glu242 is not rapidly reprotonated after the proton arrives at the PLS, a second CcO model was introduced. Here, Glu242 is deprotonated, but all other conditions are the same as in the first model. Figure 5 shows the resultant PMFs. Due to the negative charge on the glutamate, the excess proton is stabilized as it approaches Glu242. Thus, it is observed that the proton is more stabilized in the region $z_{CEC} \leq 5$ Å and more destabilized in the region $z_{CEC} \geq 10$ Å compared to the first model. However, the clear CcO oxidation state dependence is still evident. While the OO and OR states are found to inhibit the PT to the upper hydrophilic region, the RO state exhibits a much lower PT barrier. This is consistent with the mechanism shown in Figure 2 in view of the protonation state of Glu242. Note that the hydrogen-bond network is also affected by the oxidation state change (see Section 1 of the Supporting Information).

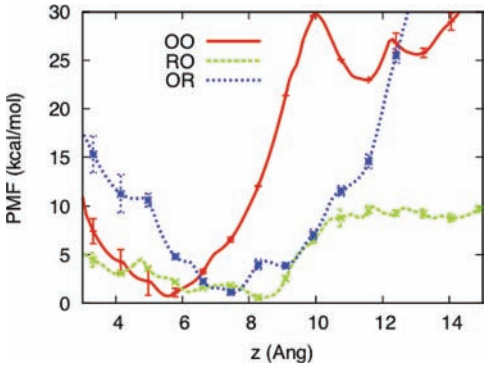

Figure 5. PT free energy profiles (PMFs) as functions of the z coordinate of the excess proton CEC for the second model. (Glu242 is deprotonated, and the BNC binds a water molecule.) The PT free energy barrier is significantly lower in the RO state than in the other two states.

A "valve" role for Glu242 was originally proposed through standard empirical MD simulations in the absence of an explicit excess proton.[33] However, it has remained unclear whether the deprotonated Glu242 can turn down toward the D-channel in the presence of an explicit excess proton in the water filled region beyond the residue and thus impede the proton flux from leaking back. Here, Figure 6 shows the probability distributions of the Glu242 orientation as a function of the explicit excess proton CEC coordinate along the post-Glu242 water-mediated pathway. (The coordinates of Glu242 were sampled every 1000 MD steps whereas the CEC coordinates were sampled every 10 MD steps, and therefore, the resolution

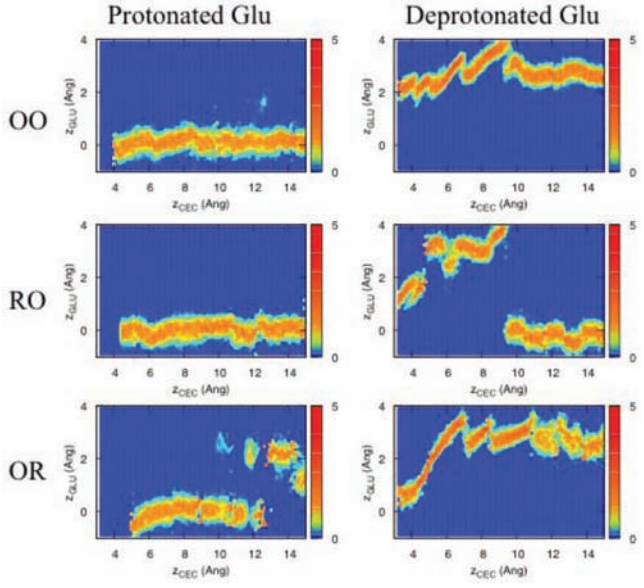

Figure 6. Probability distributions of the δ-carbon of Glu242 as a function of the z coordinate of the excess proton CEC in the region beyond the residue. (Here, z_{GLU} is the z coordinate of the δ-carbon of Glu242.) The up conformation ($z_{GLU} \sim 3$ Å) is preferable for the deprotonated Glu242 whereas the down conformation ($z_{GLU} \sim 0$ Å) is preferable for the protonated Glu242. This is due to the difference in electrostatic interaction between Glu242 and the excess protonic charge defect. When the excess proton transports away from deprotonated Glu242 in the RO state (right middle panel), it is observed that the Glu242 abruptly turns downward toward the D-channel, exhibiting a "valve" effect for Glu242.

of Figure 6 becomes slightly lower.) If Glu242 is protonated, it turns down toward the D-channel due to the electrostatic repulsion from the proton. When the proton exits from the nonpolar cavity, the up conformation of Glu242 is observed only for the OR state. If Glu242 is deprotonated and the excess proton is present inside the nonpolar cavity, the strong electrostatic attraction with the proton forces Glu242 to turn up toward the nonpolar cavity. Note that the position of the up conformation Glu242 is very sensitive to the CEC position, as in Figure 6, because in the up conformation, Glu242 forms a hydrogen bond directly to the protonated moiety in the nonpolar cavity. Importantly, however, for the RO state, it is found that Glu242 turns down (a "switch") when the excess proton exits from the nonpolar cavity, at which point the electrostatic attraction weakens (see also Figure S4 of the Supporting Information).

This result described above for the RO state provides the missing explicit evidence that the deprotonated Glu242 orientation leads to a valve effect in the RO oxidation state. After the excess proton is transported outside of the nonpolar cavity, deprotonated Glu242 turns down and is prepared to accept another proton from the D-channel. At this stage, the mean force is almost zero in the region of $z_{CEC} \geq 10$ Å. If the second proton arrives and Glu242 is reprotonated, the first proton cannot leak back easily.

Yang and Cui[36] have suggested the lipid bilayer environment plays a role in the Glu242 conformational states based on their recent empirical MD simulations, and they also showed that the protonation of PRDa3 is more dominant due to the additional proton charge. A more realistic model including the lipid bilayer may therefore be important to obtain more quantitative

dx.doi.org/10.1021/ja209176e | J. Am. Chem.Soc. 2012, 134, 1147−1152

understanding of the proton pumping mechanism in the future. However, as shown in this work and as speculated by Yang and Cui,[36] the gating of the proton transfer is regulated by the change of interaction between the protonated moiety and the redox sites of CcO. Thus, the present model can be considered as a baseline model for describing the proton pumping mechanism of CcO.

3.3. OH^--Bound CcO with Protonated Glu242. A third model was introduced in order to examine the dependence of the PT on the BNC-bound molecular species. In this model, the water molecule trapped by the BNC is replaced by the hydroxide ion (OH^-). The other conditions are the same as in the first model. This third model exactly corresponds to the E_H intermediate state, from which state CcO starts to pump the fourth proton, then reaches the R state.[3] As shown in Figure 7,

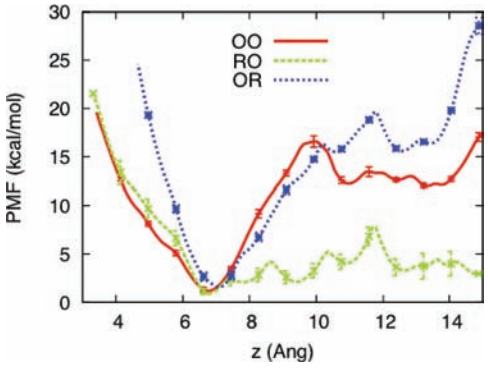

Figure 7. PT free energy profile (PMFs) as functions of the z coordinate of the excess proton CEC for the third model. (Glu242 is protonated, and the BNC binds a hydroxide.) The PT free energy barrier is significantly lower in the RO state than in the other two states.

the dependence of the PMF on the oxidation state is very similar to that of the first model, and the reduction of heme a allows the PT from the nonpolar cavity to the region above. In addition, a similar hydrogen-bond network change is observed. (See Figure S2 of the Supporting Information.) This result implies that the BNC-bound molecular species does not affect the proton behavior in this region significantly. This may be because a large amount of the negative OH^- charge is delocalized to the whole heme a_3 ring and the coordination of Cu_B changes so as to reduce the electrostatic change on the proton pathway. These results may also support a hypothesis of Wikström and co-workers[3,12] that the same proton pumping mechanism occurs in all four proton pumping processes involved in the CcO catalytic cycle.

4. CONCLUDING REMARKS

The free energy profiles (PMFs) for excess proton transport in the nonpolar cavity of CcO were calculated through reactive MS-EVB MD simulations utilizing the umbrella sampling technique. These results suggest that a "proton-switch" operates to allow the excess proton to exit from the nonpolar cavity when heme a is reduced, but not heme a_3 (the RO state). As a first step, Glu242 will turn upward and eject a proton. As the proton dissociates and travels, the deprotonated Glu242 turns down toward the D-channel and accepts a second proton, which confirms a valve effect for Glu242. Then, the proton is transported by PRDa3 to PRAa3. The electrostatic change caused by this proton transport may also be important for the electron transfer from heme a to heme a_3. Furthermore, it is found that the BNC-bound molecular species does not affect this "proton-switch" significantly, which implies that the same proton pumping mechanism can occur in all of the proton pumping processes of CcO.

The novel reactive MD simulation results presented in this paper, involving explicit descriptions of key elements of the PT process, support a proposed mechanism for CcO function,[3,11,12] while providing detailed information on its proton pumping mechanism at the molecular level.

■ ASSOCIATED CONTENT

Supporting Information

Snapshots of the characteristic hydrogen-bond networks, PMF curves for less realistic CcO models and discussion of underlying physics, and methodological details including the protonatable heme model. This material is available free of charge via the Internet at http://pubs.acs.org.

■ AUTHOR INFORMATION

Corresponding Author

gavoth@uchicago.edu

Present Address

[†]Research Center for Advanced Science and Technology, University of Tokyo.

■ ACKNOWLEDGMENTS

This research was supported by the National Institutes of Health (NIH grant R01-GM53148). The authors thank Drs. K. Wang and J. Xu for their help in the first stage of this work, and Drs. J. M. J. Swanson, C. M. Maupin, I. Sumner, and Y. Zhang for their valuable discussions and assistance. The computational resources were provided in part by the National Science Foundation via the TeraGrid computing resource. The molecular images in this article were created with the molecular graphics program VMD.[37]

■ REFERENCES

(1) Gennis, R. B. *Front. Biosci.* **2004**, *9*, 581−591.
(2) Hosler, J. P.; Ferguson-Miller, S.; Mills, D. A. *Annu. Rev. Biochem.* **2006**, *75*, 165−187.
(3) Wikström, M.; Verkhovsky, M. I. *Biochim. Biophys. Acta, Bioenerg.* **2007**, *1767*, 1200−1214.
(4) Brzezinski, P.; Johansson, A. L. *Biochim. Biophys. Acta, Bioenerg.* **2010**, *1797*, 710−723.
(5) Iwata, S.; Ostermeier, C.; Ludwig, B.; Michel, H. *Nature* **1995**, *376*, 660−669.
(6) Tsukihara, T.; Aoyama, H.; Yamashita, E.; Tomizaki, T.; Yamaguchi, H.; ShinzawaItoh, K.; Nakashima, R.; Yaono, R.; Yoshikawa, S. *Science* **1996**, *272*, 1136−1144.
(7) Mitchell, R.; Rich, P. R. *Biochim. Biophys. Acta, Bioenerg.* **1994**, *1186*, 19−26.
(8) Michel, H. *Biochemistry* **1999**, *38*, 15129−15140.
(9) Kim, Y. C.; Wikström, M.; Hummer, G. *Proc. Natl. Acad. Sci. U.S.A.* **2009**, *106*, 13707−13712.
(10) Faxén, K.; Gilderson, G.; Ädelroth, P.; Brzezinski, P. *Nature* **2005**, *437*, 286−289.
(11) Belevich, I.; Verkhovsky, M. I.; Wikström, M. *Nature* **2006**, *440*, 829−832.
(12) Kaila, V. R. I.; Verkhovsky, M. I.; Hummer, G.; Wikström, M. *Biochim. Biophys. Acta, Bioenerg.* **2009**, *1787*, 1205−1214.
(13) Wikström, M.; Verkhovsky, M. I.; Hummer, G. *Biochim. Biophys. Acta, Bioenerg.* **2003**, *1604*, 61−65.

(14) Wikström, M.; Ribacka, C.; Molin, M.; Laakkonen, L.; Verkhovsky, M.; Puustinen, A. *Proc. Natl. Acad. Sci. U.S.A.* **2005**, *102*, 10478−10481.
(15) Agmon, N. *Chem. Phys. Lett.* **1995**, *244*, 456−462.
(16) Voth, G. A. *Acc. Chem. Res.* **2006**, *39*, 143−150.
(17) Swanson, J. M. J.; Maupin, C. M.; Chen, H. N.; Petersen, M. K.; Xu, J. C.; Wu, Y. J.; Voth, G. A. *J. Phys. Chem. B* **2007**, *111*, 4300−4314.
(18) Tsukihara, T.; Shimokata, K.; Katayama, Y.; Shimada, H.; Muramoto, K.; Aoyoma, H.; Mochizuki, M.; Shinzawa-Itoh, K.; Yamashita, E.; Yao, M.; Ishimura, Y.; Yoshikawa, S. *Proc. Natl. Acad. Sci. U.S.A.* **2003**, *100*, 15304−15309.
(19) Gilderson, G.; Salomonsson, L.; Aagaard, A.; Gray, J.; Brzezinski, P.; Hosler, J. *Biochemistry* **2003**, *42*, 7400−7409.
(20) Roux, B. *Comput. Phys. Commun.* **1995**, *91*, 275−282.
(21) Tepper, H. L.; Voth, G. A. *Biophys. J.* **2005**, *88*, 3095−3108.
(22) Fadda, E.; Chakrabarti, N.; Pomès, R. *J. Phys. Chem. B* **2005**, *109*, 22629−22640.
(23) Siegbahn, P. E. M.; Blomberg, M. R. A.; Blomberg, M. L. *J. Phys. Chem. B* **2003**, *107*, 10946−10955.
(24) Kaila, V. R. I.; Sharma, V.; Wikström, M. *Biochim. Biophys. Acta, Bioenerg.* **2011**, *1807*, 80−84.
(25) Daskalakis, V.; Farantos, S. C.; Guallar, V.; Varotsis, C. *J. Phys. Chem. B* **2011**, *115*, 3648−3655.
(26) Ghosh, N.; Prat-Resina, X.; Gunner, M. R.; Cui, Q. *Biochemistry* **2009**, *48*, 2468−2485.
(27) Johansson, A. L.; Chakrabarty, S.; Berthold, C.; Högbom, M.; Warshel, A.; Brzezinski, P. *Biochim. Biophys. Acta* **2011**, *1807*, 1083−1094.
(28) Chakrabarty, S.; Namslauer, I.; Brzezinski, P.; Warshel, A. *Biochim. Biophys. Acta, Bioenerg.* **2011**, *1807*, 413−426.
(29) Pisliakov, A. V.; Sharma, P. K.; Chu, Z. T.; Haranczyk, M.; Warshel, A. *Proc. Natl. Acad. Sci. U.S.A.* **2008**, *105*, 7726−7731.
(30) Maupin, C. M.; Aradi, B.; Voth, G. A. *J. Phys. Chem. B* **2010**, *114*, 6922−6931.
(31) Goyal, P.; Elstner, M.; Cui, Q. *J. Phys. Chem. B* **2011**, *115*, 6790−6805.
(32) Yamashita, T.; Voth, G. A. *J. Phys. Chem. B* **2010**, *114*, 592−603.
(33) Kaila, V. R. I.; Verkhovsky, M. I.; Hummer, G.; Wikström, M. *Proc. Natl. Acad. Sci. U.S.A.* **2008**, *105*, 6255−6259.
(34) Maréchal, A.; Rich, P. R. *Proc. Natl. Acad. Sci. U.S.A.* **2011**, *108*, 8634−8638.
(35) Xu, J.; Voth, G. A. *Biochim. Biophys. Acta, Bioenerg.* **2008**, *1777*, 196−201.
(36) Yang, S.; Cui, Q. *Biophys. J.* **2011**, *101*, 61−69.
(37) Humphrey, W.; Dalke, A.; Schulten, K. *J. Mol. Graph.* **1996**, *14*, 33−38.